metals

MDPI

Article

Nonlinear Ultrasonic Guided Wave Method Using Semi-Analytical Finite Element (SAFE) Technique on a Damaged SWO-V Spring Coil

Jeongnam Kim [1], Junpil Park [2], Bo Zhu [3] and Younho Cho [4,*]

[1] Graduate School, School of Mechanical Engineering, Pusan National University, Busan 46241, Korea; kjnnoah@pusan.ac.kr
[2] Institute of Nuclear Safety and Management, Pusan National University, Busan 46241, Korea; jpp@pusan.ac.kr
[3] Department of Pipeline In-Line Inspection, Shandong Special Equipment Inspection Institute Co. Ltd., Jinan 250101, China; zbhenry2015@126.com
[4] School of Mechanical Engineering, Pusan National University, Busan 46241, Korea
* Correspondence: mechcyh@pusan.ac.kr; Tel.: +82-051-510-2323

Abstract: This work presents a non-destructive method for quantitative essessment of fatigue damage of materials with linear elastic properties using nonlinear ultrasonic techniques. A nonlinear study was conducted on these materials with fatigue and shot peening processing using a nonlinear ultrasonic technique. A numerical method based on the semi-analytical finite element (SAFE) technique, was used to obtain the phase-matching modes of the specimens. Experiments confirm that the nonlinearity for shot peening and samples with a certain level of fatigue shows a tendency to increase with levels of fatigue.

Keywords: nonlinear guided wave; SAFE; materials with linear elastic properties; phase matching mode; fatigue; shot peening

Citation: Kim, J.; Park, J.; Zhu, B.; Cho, Y. Nonlinear Ultrasonic Guided Wave Method Using Semi-Analytical Finite Element (SAFE) Technique on a Damaged SWO-V Spring Coil. *Metals* **2021**, *11*, 752. https://doi.org/10.3390/met11050752

Academic Editor: Jean-Michel Bergheau

Received: 1 March 2021
Accepted: 17 April 2021
Published: 2 May 2021

1. Introduction

Driving Safety is seriously affected by malfunction or damage of materials with linear elastic properties, such as tension rods, ton-shoulders, and springs used in vehicles. Research on the safety of the structure and research on the optimization and weight reduction of parts are becoming more important. Therefore, research on these materials is of a great concern.

In general, the life evaluation of materials with linear elastic properties is performed through the Nakamura fatigue test, which is one of the destructive evaluation techniques. However, this technique consumes considerable time and cost. In addition to life evaluation, to improve the durability, life, and performance of a spring, a cold working process called shot peening is performed on these materials. Shot peening leads to plastic deformation on the surface and changes the mechanical properties of the material. Surface cracks do not propagate well in materials subjected to compressive stress, so the propagation of micro-cracks on the surface of the material can be prevented through shot peening.

In addition, the plastic deformation caused by shot peening results in residual compressive stress on the surface and can impart resistance to metal fatigue and some forms of stress corrosion. However, if residual stress is generated while impurities are contained within the material, it may break along grain boundaries that are weakened by impurities. Currently, preventing the accidents induced by damaged springs becomes a significant issue, and the soundness of spring coils has a great influence on vehicle performance and reliability. Therefore, it is necessary to strictly apply safety management of a structure before an accident occurs, and to improve the life evaluation by detecting micro-cracks or defects in an early stage by a non-destructive method.

For life evaluation and safety management, a nonlinear guided wave technique can be used. It has been explored for many years as a promising tool that can diagnose micro-defects or microscopic structural changes in micro-and nano-units through the selection of various guided wave modes [1,2]. Buck et al. [3] conducted a study on stress and changes in the second harmonic function. Later, Jacobs and colleagues [4] studied the plasticization of materials using nonlinear ultrasonic guided waves [5–13]. They investigated the nonlinear shear horizontal wave and the cumulative second harmonic.

Guided waves were applied to efficiently inspect slender samples such as wire rods [14,15]. Gazis performed basic ultrasonic guided wave analysis on cylindrical structures [16]. Other related research was mainly studied by Rose and Cowley [17,18]. Recently, Cho et al. conducted an inspection by using a PVDF sensor to detect localized fatigue damage on an aluminum plate [19]. Guan and Su compared the differences in fatigue crack detection using nonlinear guided ultrasound between plate and pipe structures [20]. Li et al. conducted a nonlinear guided ultrasonic assessment of laminated composites subjected to low-speed impact and improved the signal-to-noise ratio (S/N ratio) by using a phase inversion method to measure the second harmonic [21]. Recently, many researchers have conducted research on the relationship between nonlinearity and linear elastic materials such as pipes using advanced technology [22–24].

This study presents an experimental approach to assess the local micro-grain structure change of materials with linear elastic properties based on the nonlinear features corresponding to the damage. In linear elasticity, there is a proportional constant representing the slope of a straight line relating with load and deformation. For example, in the case of a simple unidirectional tensile test, the slope between the axial stress and the corresponding axial strain is expressed as Young's modulus E, and this is one of the linear elastic moduli. It is a well-known fact that when a material is subjected to microdamage, such as grain structure change, the slope tends to show a tiny nonlinearity. The nonlinearity can be linked to the higher harmonic amplitude of ultrasound, providing a specific feature of the corresponding microdamage. NDE was performed for a wire rod specimen subjected to shot peening using the nonlinear guided ultrasonic method in the comparison of the Nakamura fatigue test. In this study, the second harmonic of the longitudinal wave was generated, and the reliability of the experimental result was confrimed by controlling the fatigue variables.

2. Theoretical Background

2.1. Nonlinear Wave Theory

When the higher-order elastic constants of solid materials increase, the relationship of stress and strain is nonlinear rather than linear. With linear ultrasonic theory, it is difficult to describe the behavior of a material that does not follow the plastic region or elastic motion of the stress-strain curve, but applying nonlinear supersonic theory allows for more accurate behavior [25]. In the nonlinearity measurement method, ultrasonic waves of a single frequency are incident on the sample and propagate for a certain distance. The signal is distorted due to the third-order modulus of elasticity of the material, which is considered to be the second harmonic. The second harmonic occurs when there is a change in micro-structure [26], such as plastic deformation and corrosion, and it is relatively small compared to the first harmonic.

The nonlinear factor indicates the relationship between the microstructural changes of these materials and the denominator and is defined by Equation (1):

$$\beta_l = -(3 + \frac{C_{111}}{\rho c_l^2}) = \frac{A_2}{A_1^2}\frac{8}{k^2 x} \quad (1)$$

where C_{111} is the cubic elastic modulus, c_l is the velocity of the longitudinal wave, ρ is the density of the material, and A_1 and A_2 are the amplitude of the primary and second harmonic, respectively. k is the wave number, and x is distance of the propagation. Under

certain conditions, the parameter β is measured for a fixed wavenumber and propagation distance:

$$\beta' = \frac{A_2}{A_1^2} \propto \beta \tag{2}$$

2.2. General Solution of Nonlinear Wave Equation in a Solid Cylindrical Rod

To obtain a general solution for a nonlinear wave equation in a solid cylindrical rod, elastic waveguides with an arbitrary cross-section area are theoretically studied. The harmonic generation of ultrasonic guided wave propagation in cylindrical rods was reported by de Lima et al. [12]. Practically, in tube-like structures, the guided wave propagation provides a more efficient approach to detect material nonlinearity due to its lower energy diffusion [27].

In Lagrangian coordinates, the nonlinear wave equation is expressed as in Equation (3):

$$(\lambda + 2\mu)\nabla(\nabla \cdot u) - \mu\nabla \times (\nabla \times u) + f = \rho_0 \frac{\partial^2 u}{\partial t^2} \tag{3}$$

where u is the particle displacement, λ and μ are the Lamé constants, ρ_0 is the initial density of the material, and $f(u)$ is the nonlinear term. The perturbation method is used to solve the nonlinear wave equation, and the solution is taken from Equation (4):

$$u = u_1 + u_2 \tag{4}$$

where u_1 is the primary wave, u_2 is the second harmonic (double frequency component), and u_2 is assumed to be much smaller than u_1. The primary wave with frequency ω and the wavenumber k is written as in Equation (5):

$$u_1 = u(r)e^{i(kz-\omega t)} \tag{5}$$

Constructing the second-order solution using model expansion [21], the total second-harmonic field can be written as Equation (6):

$$\begin{aligned} u_2 &= \tfrac{1}{2}\sum_{m=1}^{\infty} A_m(z)u_{(2,m)}(r)e^{-i2\omega t} \\ v_2 &= \tfrac{1}{2}\sum_{m=1}^{\infty} A_m(z)v_{(2,m)}(r)e^{-i2\omega t} \\ s_2 &= \tfrac{1}{2}\sum_{m=1}^{\infty} A_m(z)s_{(2,m)}(r)e^{-i2\omega t} \end{aligned} \tag{6}$$

where $u(2,m)$ is the displacement field function. $v = \frac{du}{dt}$ and $v(2,m)$ are the particle velocity, and $s(2,m)$ is the stress tensor for the mth double frequency components. r is the thickness of the waveguide. $A_m(z)$ is the modal amplitude:

$$A_m = \overline{A}_m(z)e^{i2kz} - \overline{A}_m(0)e^{ik_n^* z} \tag{7}$$

$A_m(z)$ is the solution of the following ordinary differential Equation (8) with the condition $u_2 = 0$ at $z = 0$:

$$4p_{mn}\left(\frac{d}{dz} - ik_n^*\right)A_m(z) = (f_n^{surf} + f_n^{vol})e^{i2kz} \tag{8}$$

where:

$$\begin{aligned} p_{mn} &= -\tfrac{1}{4}\textstyle\int_\Omega (v_n^* \cdot s_m + v_m \cdot s_n^*) \cdot n_z d\Omega \\ f_n^{surf}(z) &= \textstyle\int_\Gamma v_n^* \cdot s^{2\omega} \cdot n_z d\Gamma \\ f_n^{vol}(z) &= \textstyle\int_\Omega v_n^* \cdot f^{2\omega} d\Omega \end{aligned} \tag{9}$$

In Equation (9), Ω is the waveguide cross-sectional area and Γ is the curve enclosing Ω. The terms f_n^{surf} and f_n^{vol} are respectively defined as the complex external power due to the surface traction $s^{2\omega}$ and the volume force $f^{2\omega}$. k_n is the wavenumber of the mode identified by index n, which is not orthogonal ($p_{mn} \neq 0$) to the mode with wave number k_m.

This analysis is applied to a cross-sectional area of any shape. For the cylindrical rod shown in Figure 1, the expressions of p_{mn}, f_n^{surf}, and f_n^{vol} are [12]:

$$\begin{aligned} p_{mn} &= -\tfrac{1}{16}\int_0^{2\pi}\int_0^b [v_m^*(r,\theta)\cdot s_n(r,\theta) + v_n(r,\theta)\cdot s_m^*(r,\theta)]\cdot n_z r\,dr\,d\theta \\ f_n^{\text{surf}}(z) &= -\tfrac{b}{2}\int_0^{2\pi} v_n^*(b,\theta)\cdot s^{2\omega}(b,\theta)\cdot n\,d\theta \\ f_n^{\text{vol}}(z) &= \tfrac{1}{2}\int_0^b\int_0^{2\pi} v_m^*(r,\theta)\cdot f^{2\omega}(r,\theta) r\,dr\,d\theta \end{aligned} \tag{10}$$

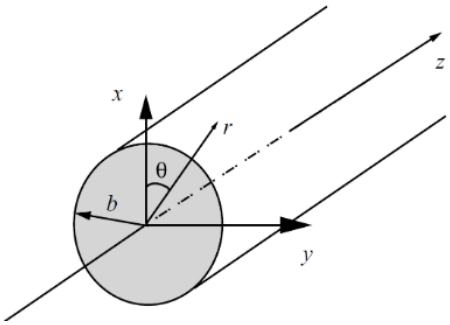

Figure 1. Diagram of cylindrical waveguide rod.

The assumed primary wavefield of particle displacement components is [26]:

$$\begin{aligned} u_1^r &= u_r(r)\cos(n\theta)e^{i(kz-\omega t)} \\ u_1^\theta &= u_\theta(r)\sin(n\theta)e^{i(kz-\omega t)} \\ u_1^z &= u_z(r)\cos(n\theta)e^{i(kz-\omega t)} \end{aligned} \tag{11}$$

where the circumferential order is n = 0, 1, 2, $\cdots$. For axis-symmetric modes, n = 0 and $n \geq 1$ for the flexural modes. Generally, the terms u_1^r, u_1^θ, and u_1^z depend on the type of waveguide and family of modes.

In practice, second harmonic generation with an accumulative effect is of great interest. The reason is that the cumulative effect of the second harmonic amplitude has a great advantage for detection in experimental work to measure the nonlinear effect with a sufficient signal-to-noise ratio. From the analysis, specific conditions must be satisfied for second harmonic generation with accumulative effect [3,14,28].

1. Nonzero power flux from the primary to the secondary wave: $f_n^{\text{surf}} + f_n^{\text{vol}} \neq 0$;
2. Matching phase and group velocities require equal phase and group velocities of the primary and the secondary waves when $k_n^* = 2k$ (synchronism).

2.3. Phase Matching Mode

Due to the dispersion and multi-mode characteristics of guided ultrasound, it is difficult to efficiently generate the second harmonic. Therefore, one of the numerical analysis methods, the SAFE technique, was used to induce the phase-matching mode of the longitudinal wave mode of the specimen. Figure 2 shows a SAFE model of a rod.

$$\begin{aligned} u &= \begin{bmatrix} u_\theta & u_r & u_z \end{bmatrix}^T \\ \sigma &= \begin{bmatrix} \sigma_\theta & \sigma_r & \sigma_z & \tau_{rz} & \tau_{z\theta} & \tau_{\theta r} \end{bmatrix}^T \\ \varepsilon &= \begin{bmatrix} \varepsilon_\theta & \varepsilon_r & \varepsilon_z & \gamma_{rz} & \gamma_{z\theta} & \gamma_{\theta r} \end{bmatrix}^T = Lu \end{aligned} \tag{12}$$

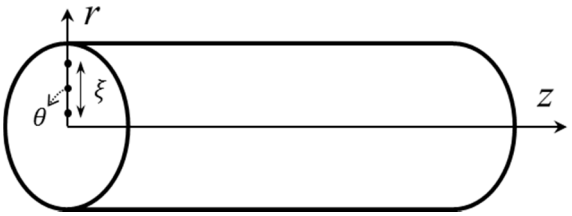

Figure 2. SAFE model of rod in cylindrical coordinates.

In Equation (12), T is the transpose of the matrix, and the differential operator L in the cylindrical coordinate system is:

$$L = \begin{bmatrix} \frac{1}{r}\partial\theta & 0 & 0 & 0 & \partial z & \partial r - \frac{1}{r} \\ \frac{1}{r} & \partial r & 0 & \partial z & 0 & \frac{1}{r}\partial\theta \\ 0 & 0 & \partial z & \partial r & \frac{1}{r}\partial\theta & 0 \end{bmatrix} \tag{13}$$

The relationship between strain and displacement is expressed as Equation (14):

$$\varepsilon = b_1 u_z + b_2 u_r + b_3 \frac{1}{r} u_\theta + b_4 \frac{1}{r} u \tag{14}$$

where b_1, b_2, b_3, and b_4 are:

$$\begin{aligned} b_1 &= \begin{bmatrix} 0 & 0 & 0 \\ 0 & 0 & 0 \\ 0 & 0 & 1 \\ 0 & 0 & 0 \\ 1 & 0 & 0 \\ 0 & 1 & 0 \end{bmatrix}, \; b_2 = \begin{bmatrix} 0 & 0 & 0 \\ 0 & 1 & 0 \\ 0 & 0 & 0 \\ 1 & 0 & 0 \\ 0 & 0 & 0 \\ 0 & 0 & 1 \end{bmatrix}, \\ b_3 &= \begin{bmatrix} 1 & 0 & 0 \\ 0 & 0 & 0 \\ 0 & 0 & 0 \\ 0 & 0 & 0 \\ 0 & 0 & 1 \\ 0 & 1 & 0 \end{bmatrix}, \; b_4 = \begin{bmatrix} 0 & 1 & 0 \\ 0 & 0 & 0 \\ 0 & 0 & 0 \\ 0 & 0 & 0 \\ 0 & 0 & 0 \\ -1 & 0 & 0 \end{bmatrix} \end{aligned} \tag{15}$$

Figure 3 shows a method of performing discretization along the radial direction using a one-dimensional three-node element. The shape function is an interpolation function defined as Equation (16):

$$N_1 = \frac{\xi^2 - \xi}{2}, \; N_2 = 1 - \xi^2, \; N_3 = \frac{\xi^2 + \xi}{2} \tag{16}$$

The displacement field of each discrete element is described as a shape function matrix and a node displacement vector after finite element discretization.

$$U^{(e)} = N q^{(e)} e^{i(kz + m\theta - \omega t)} \tag{17}$$

In Equation (17), m is the circumferential order. The shape function is:

$$N = \begin{bmatrix} N_1 & 0 & 0 & N_2 & 0 & 0 & N_3 & 0 & 0 \\ 0 & N_1 & 0 & 0 & N_2 & 0 & 0 & N_3 & 0 \\ 0 & 0 & N_1 & 0 & 0 & N_2 & 0 & 0 & N_3 \end{bmatrix} \tag{18}$$

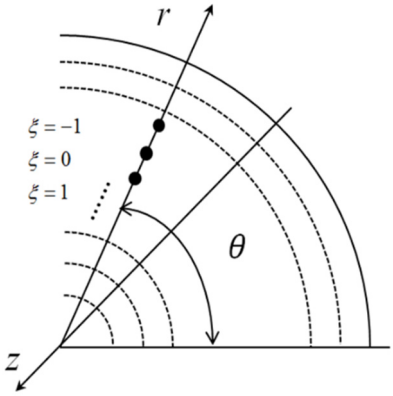

Figure 3. Discretization of a pipe with 1D three-node elements.

Since each node has 3 degrees of freedom (DOFs) in different directions, the vector $q^{(e)}$ is denoted as Equation (19):

$$q^{(e)} = \left[\begin{array}{cccccccccc} U_{\theta 1} & U_{r1} & U_{z1} & U_{\theta 2} & U_{r2} & U_{z2} & U_{\theta 3} & U_{r3} & U_{z3} \end{array} \right]^T \tag{19}$$

Therefore, the strain can be expressed as Equations (20) and (21):

$$\varepsilon = b_1 N(\xi)\partial_z q^{(e)} e^{i(kz+m\theta-\omega t)} + \frac{1}{r_\xi} b_2 \partial_\xi N(\xi) q^{(e)} e^{i(kz+m\theta-\omega t)} + b_3 \frac{1}{r} N(\xi) q^{(e)} e^{i(kz+m\theta-\omega t)} + b_4 \frac{im}{r} N(\xi) q^{(e)} e^{i(kz+m\theta-\omega t)} \tag{20}$$

$$\varepsilon^{(e)} = (B_1 + ikB_2) q^{(e)} e^{i(kz+m\theta-\omega t)} \tag{21}$$

Here, the geometric matrix B_1 is:

$$\begin{array}{l} B_1 = \frac{1}{r_\xi} b_2 N_\xi + b_3 \frac{1}{r} N + b_4 \frac{im}{r} N, \\ B_2 = b_1 N \end{array} \tag{22}$$

N is the derivative term of the shape function matrix for the e-direction in the local coordinate system. By applying the traction-free boundary condition for the SAFE model, the guided ultrasound equation for the wave motion of each element can be obtained based on Hamilton's principle [29,30]:

$$(k_1^{(e)} + i\xi k_2^{(e)} + \xi^2 k_3^{(e)} - \omega^2 m^{(e)}) \mathrm{U}^{(e)} = 0 \tag{23}$$

where:

$$\begin{array}{l} k_1^{(e)} = \int\limits_{\Omega_e} B_1^T \widetilde{C}_e B_1 \mathrm{d}\Omega_e, \, k_2^{(e)} = \int\limits_{\Omega_e} (B_1^T \widetilde{C}_e B_2 - B_2^T \widetilde{C}_e B_1) \mathrm{d}\Omega_e, \\ k_3^{(e)} = \int\limits_{\Omega_e} B_2^T \widetilde{C}_e B_2 \mathrm{d}\Omega_e, \, m^{(e)} = \int\limits_{\Omega_e} N^T \rho_e N \mathrm{d}\Omega_e \end{array} \tag{24}$$

A standard finite element assembly for all elements can be simplified to a common eigenvalue problem in the global coordinate system as in Equation (25):

$$(k_1 + i\xi k_2 + \xi^2 k_3 - \omega^2 m)_M \mathrm{U} = 0 \tag{25}$$

It can also be marked as a first-order native system as in Equation (26):

$$[A - kB]_{2M} Q = 0 \tag{26}$$

where:

$$A = \begin{bmatrix} 0 & k_1 - \omega^{2M} \\ k_1 - \omega^{2M} & \hat{k}_2 \end{bmatrix}, B = \begin{bmatrix} k_1 - \omega^{2M} & 0 \\ 0 & -k_3 \end{bmatrix}, \quad Q = \begin{bmatrix} \hat{U} \\ k\hat{U} \end{bmatrix} \tag{27}$$

Given the frequency values of the wave model, a series of wavenumbers can be calculated by solving this typical eigenvalue problem. The dispersion relationship can be derived later.

3. Experiment Setup

3.1. Material Properties

The material properties of the specimen are shown in Tables 1 and 2 [31]. The phase and group velocity dispersion curves of the longitudinal mode are shown in Figure 4. This information can be obtained directly by replacing this information with the SAFE code. Single-frequency and double-frequency dispersion diagrams are indicated by solid and dotted lines, respectively.

Table 1. Material properties of the SWO-V specimen.

Items	Values
Poisson's ratio	0.35
Elastic modulus (GPa)	205
Density (Kg/m^3)	7850
Diameter (mm)	3.1

Table 2. Chemical composition and material property of the SWO-V specimen.

The Chemical Compositions of Rod Material: SWO-V (Mass %)					
C	Mn	Si	P	S	Cu
0.60–0.75	0.60–0.90	0.12–0.32	Under 0.025	Under 0.025	Under 0.02

3.2. Experimental Design

In Figure 4, it can be seen that the same values of the phase and group velocity appeared in the red region. Therefore, 1.4 MHz in mode L (0,2) and 2.8 MHz in L (0,3) were selected. Figure 5 shows a diagram of the experimental setup. The tone burst ultrasonic device was a RITEC PRP-4000, which was used to generate and receive ultrasonic waves. The transducer and the acrylic wedge generated longitudinally induced ultrasonic waves, and the angle of incidence was derived by Snell's law [32]:

$$\theta = \sin^{-1} \frac{c_{\text{acrylic}}}{c_p} \tag{28}$$

In this equation, c_{acrylic} = 2670 m/s is the propagation velocity of ultrasonic waves in acrylic, c_p = 6500 m/s is the phase velocity in L (0,2) mode at 1.4 MHz, and theta is the incident angle. The diameter of the specimen is 3.1 mm, and it was cut to a length of 946 mm. Shot peening was performed for 40 min with a 0.6 mm diameter shot ball made of SWRH82A and then shot peening was performed again with a 0.3 mm shot ball.

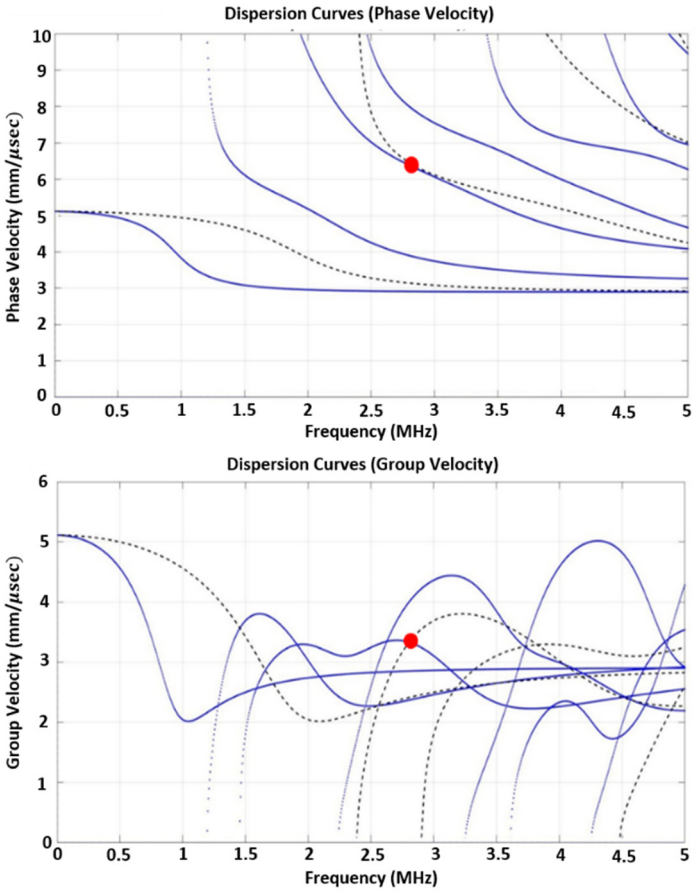

Figure 4. Numerical L mode dispersion curves of the specimen based on the SAFE technique.

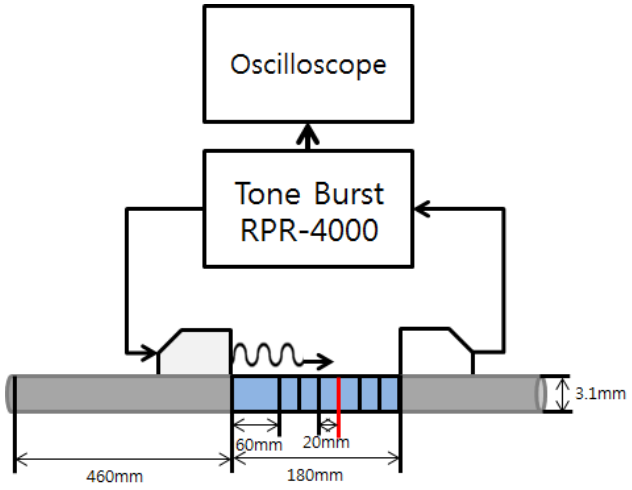

Figure 5. Diagram of second harmonic wave testing method.

3.3. Experimental Set Up

As seen in Figure 5, the signal was generated at a distance of 460 mm from the end of the sample and received at intervals of 20 mm from a distance of 60 mm. A total of 7 sections were inspected, including the center of the specimen. Each section was measured 5 times. The total length of the flaw was 180 mm, and the area where the maximum fatigue stress occurred was inspected. The signal was measured to investigate the correlation of the nonlinearity according to the degree of fatigue. A signal in longitudinal mode was generated for the specimen using the RITEC RPR-4000 tone burst ultrasonic device.

As shown in Figure 6, a motor was installed at the left end of the rod, and a fatigue test was conducted by supporting the other end of the rod [33]. While the test was being carried out, the largest load was applied to the center of the specimen. A separate recording device was connected to the device, and the number of rotations until the rod was damaged during the experiment was recorded. In this study, to manufacture damaged specimens due to fatigue load, fatigue tests were conducted by dividing the degree of fatigue into 4 types. The number of revolutions per minute was 5000 rpm, and based on 100% being 10 million cycles, 0% (0 cycle), 30% (3 million cycles), 60% (6 million cycles), 100% (10 million cycles), 130% (13 million cycles), and 160% (16 million cycles) were applied. Michihiko (1992) also showed the result of the test with the number of cycles up to 10^7 for SWO-V during the Nakamura fatigue test. Therefore, in this paper, 10^7 cycles were the 100% standard [34].

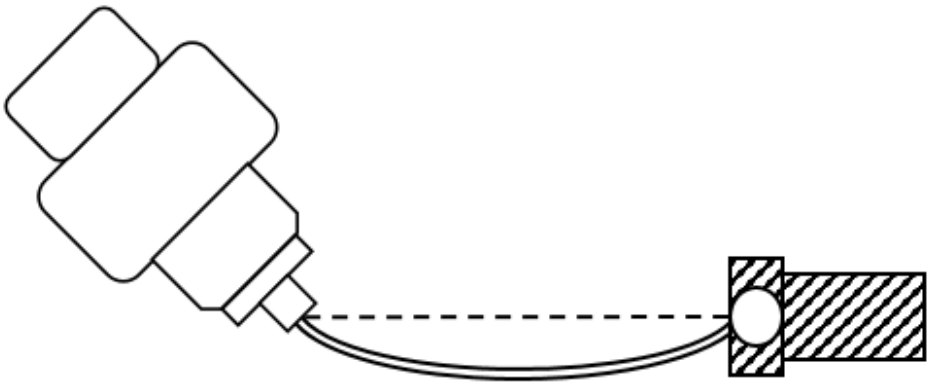

Figure 6. Diagram of Nakamura fatigue test with the rotating-bending machine.

4. Results

Figure 7 shows the typical waveform of the received signal, and Figure 8 shows its spectrum. The received signal was processed in the frequency domain using a Fast Fourier Transform (FFT) to obtain the spectrum. The nonlinear parameters were calculated by taking values from the spectrum of the fundamental frequency (1.4 MHz) and the second harmonic frequency.

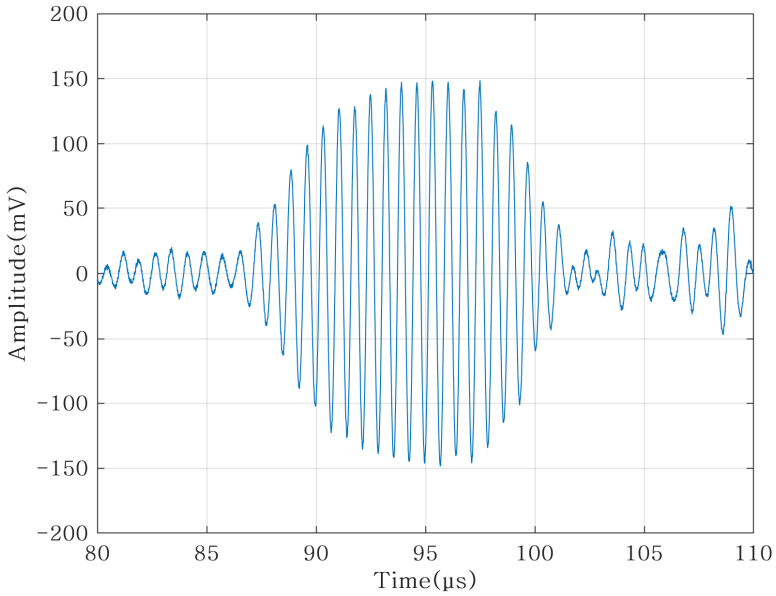

Figure 7. The received signal: time domain waveform.

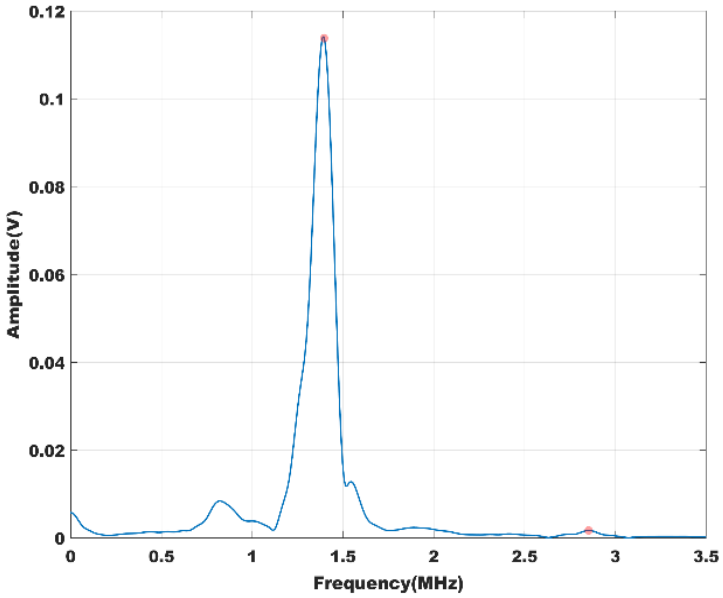

Figure 8. The received signal for Fourier spectra of the fundamental and second harmonic signal.

Figure 9 shows the nonlinear result of shot peening. For the two specimens, it was confirmed that the nonlinearity increased with the distance, and the nonlinearity was dominantly influenced by the overlapping effect. However, the nonlinearity of the shot peening specimen marked with a red dotted line was higher by about 0.5 to 1 than that of the general specimen marked with a solid black line. Although there is a slight difference in nonlinearity, it could be seen that in shot peening and general specimens, the nonlinearity tended to increase as the measurement distance increased.

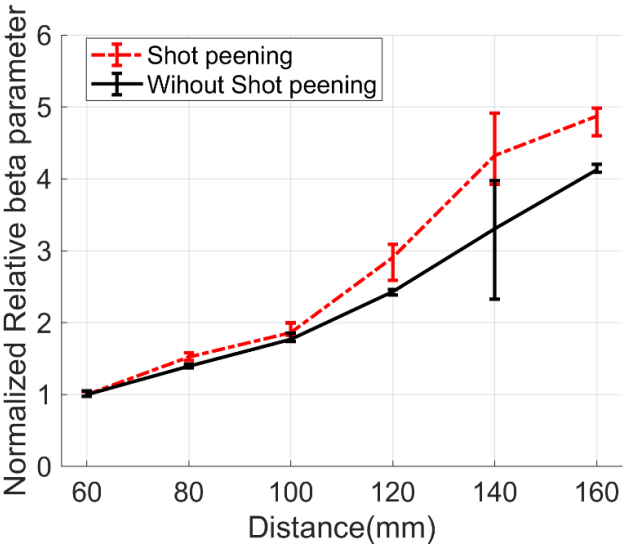

Figure 9. Nonlinearity with shot peening and without shot peening.

The results of the nonlinear experiment according to the degree of fatigue are shown in Figure 10. For the specimen (0%) not subjected to the fatigue test, it was confirmed that the nonlinearity increased as the measurement distance increased, and the overlapping effect was dominantly affected. For specimens with a fatigue degree of 30% to 100%, the nonlinear tendency was dominated by the superposition effect. The degree of fatigue was a nonlinear result for 130% and 160% specimens. With a specimen with a degree of fatigue exceeding 10 million times, and it can be seen that the nonlinear tendency gradually decreased from around 120 mm, the point where the fatigue load was the largest.

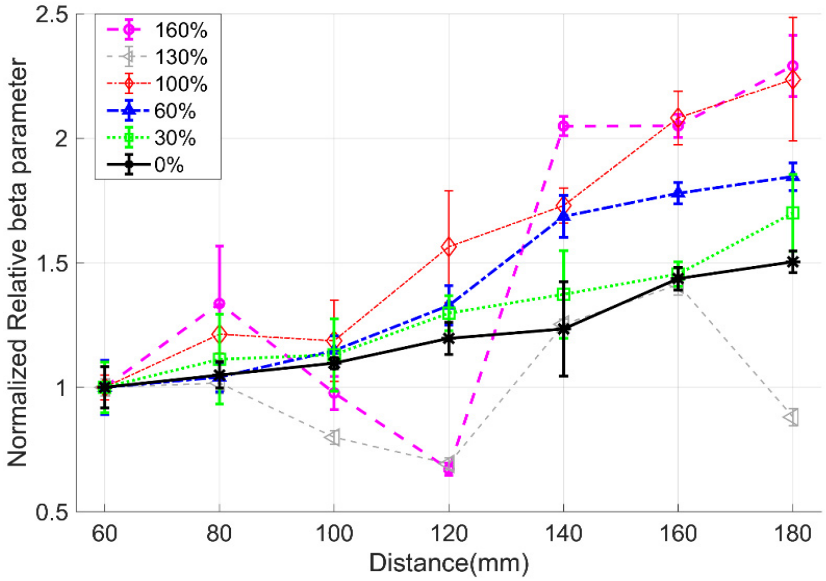

Figure 10. Nonlinearity for fatigue-damaged spring rods.

5. Conclusions

In this study, a SAFEM was used to calculate the dispersion curve of a guided ultrasonic wave. One of the NDT methods, the nonlinear guided ultrasonic flaw detection method, was used to investigate the nonlinear tendency of a shot peening specimen according to the surface change, and it was confirmed that the nonlinear tendency increase when the sub surface grain structure changed due to the shot peening. For the specimens subjected to the Nakamura fatigue test, in the case of 0% to 100%, the damping effect was not large, so nonlinearity was dominant; however, when the fatigue cycle exceed the fatigue limit, plastic deformation occurres relatively greater attenuation. In Figure 10, the 120 mm point was the point where the fatigue load was the largest of the length of the specimen, and since the plastic deformation occurred the most, it was estimated that the nonlinearity decreased in the experimental results of 130% and 160%. This was assumed to be the result of plastic deformation in the microstructure due to fatigue.

Author Contributions: Conceptualization, J.K. and Y.C.; methodology, J.K.; software, B.Z.; validation, J.K. and Y.C.; formal analysis, J.K. and J.P.; investigation, J.K. and B.Z.; resources, Y.C.; data curation, J.K.; writing—original draft preparation, J.K.; writing—review and editing, B.Z., J.P. and Y.C.; visualization, J.K.; supervision, Y.C.; project administration, Y.C.; funding acquisition, Y.C. All authors have read and agreed to the published version of the manuscript.

Funding: This work was supported by the National Research Foundation of Korea (NRF) grant and funded by the Korean government (MSIT) (grant no. NRF-2020M2D2A02069933).

Acknowledgments: This research was carried out with the support of materials from DAEWON KANG UP CO., LTD., Haman 52061, Korea.

Conflicts of Interest: The authors declare no conflict of interest.

References

1. Bermes, C.; Kim, J.Y.; Qu, J.; Jacobs, L.J. Experimental characterization of material nonlinearity using Lamb waves. *Appl. Phys. Lett.* **2007**, *90*, 021901. [CrossRef]
2. Nagy, P.B. Fatigue damage assessment by nonlinear ultrasonic material characterization. *Ultrasonics* **1998**, *36*, 275–381. [CrossRef]
3. Buck, O. Harmonic generation for measurement of internal stress as produced by dislocation. *IEEE Trans. Sonics Ultrason.* **1976**, *23*, 346–350. [CrossRef]
4. Kim, J.Y.; Qu, J.; Jacobs, L.J. Acoustic nonlinearity parameter due to micro-plasticity. *J. Nondestruct. Eval.* **2006**, *25*, 29–37. [CrossRef]
5. Li, W.; Cho, Y.; Achenbach, J.D. Detection of thermal fatigue in composites by second harmonic Lamb waves. *Smart Mater. Struct.* **2012**, *21*, 085019. [CrossRef]

6. Li, W.; Choi, J.; Cho, Y. Second Harmonic Generation of Shear Horizontal Guided Wave Propagation in Plate-like structures. *Phys. Procedia* **2015**, *70*, 451–454. [CrossRef]
7. Park, J.; Lee, J.; Min, J.; Cho, Y. Defects Inspection in Wires by Nonlinear Ultrasonic-Guided Wave Generated by Electromagnetic Sensors. *Appl. Sci.* **2020**, *10*, 4479. [CrossRef]
8. Deng, M. Cumulative second-harmonic generation accompanying nonlinear shear horizontal mode propagation in a solid plate. *J. Appl. Phys.* **1998**, *84*, 3500–3505.
9. Deng, M.; Liu, Z. Modal analysis of second-harmonic generation of shear horizontal modes in an elastic plate. *Appl. Phys. Lett.* **2002**, *81*, 1916–1918. [CrossRef]
10. Deng, D. Analysis of second-harmonic generation of Lamb modes using a modal analysis approach. *J. Appl. Phys.* **2003**, *94*, 4152. [CrossRef]
11. De Lima, W.J.; Hamilton, M.F. Finite-amplitude waves in isotropic elastic plates. *J. Sound Vib.* **2003**, *265*, 819–839. [CrossRef]
12. De Lima, W.J.; Hamilton, M.F. Finite-amplitude waves in isotropic elastic waveguides with arbitrary constant cross-sectional area. *Wave Motion* **2006**, *41*, 1–11. [CrossRef]
13. Kim, J.; Zhu, B.; Cho, Y. An experimental study on second harmonic generation of guided wave in fatigued spring rod. *J. Mech. Sci. Technol.* **2019**, *33*, 4105–4109. [CrossRef]
14. Li, W.; Deng, M.; Cho, Y. Cumulative Second Harmonic Generation of Ultrasonic Guided Waves Propagation in Tube-Like Structure. *J. Comput. Acoust.* **2016**, *24*, 1650011. [CrossRef]
15. Kim, J.; Jacobs, L.J.; Qu, J. Experimental characterization of fatigue damage in a nickel-base superalloy using nonlinear ultrasonic waves. *J. Acoust. Soc. Am.* **2006**, *120*, 1266. [CrossRef]
16. Gazis, D.C. Three-dimensional investigation of the propagation of waves in hollow circular cylinders. 1. Analytical foundation. *J. Acoust. Soc. Am.* **1959**, *31*, 568–573. [CrossRef]
17. Rose, J.L. A baseline and vision of ultrasonic guided wave inspection potential. *J. Pres. Ves. Tech.* **2002**, *124*, 273–282. [CrossRef]
18. Lowe, M.J.S.; Alleyne, D.N.; Cawley, P. Defect detection in pipes using guided waves. *Ultrasonics* **1998**, *36*, 147–154. [CrossRef]
19. Cho, H.J.; Hasanian, M.; Shana, S.; Lissenden, C.J. Nonlinear guided wave technique for localized damage detection in plates with surface-bonded sensors to receive Lamb waves generated by shear-horizontal wave mixing. *NdtE Int.* **2019**, *102*, 35–46. [CrossRef]
20. Guan, R.; Lu, Y.; Wang, K.; Su, Z. Fatigue crack detection in pipes with multiple mode nonlinear guided waves. *Struct. Health Monit.* **2019**, *18*, 180–192. [CrossRef]
21. Li, W.; Jiang, C.; Qing, X.; Liu, L.; Deng, M. Assessment of low-velocity impact damage in composites by the measure of second-harmonic guided waves with the phase-reversal approach. *Sage J.* **2020**, *103*, 1–14. [CrossRef]
22. Yeung, C.; Tai Ng, C. Nonlinear guided wave mixing in pipes for detection of material nonlinearity. *J. Sound Vib.* **2020**, *485*, 115541. [CrossRef]
23. Lowe, P.; Lais, H.; Paruchuri, V.; Gan, T. Application of Ultrasonic Guided Waves for Inspection of High Density Polyethylene Pipe Systems. *Sensors* **2020**, *20*, 3184. [CrossRef] [PubMed]
24. Guan, R.; Lu, T.; Zou, F.; Wang, K.; Su, Z. A simplified analytical model for the investigation of contact acoustic nonlinearity in pipe structures. *Int. J. Mech. Sci.* **2021**, *197*, 06328. [CrossRef]
25. Li, W.; Chen, B.; Qing, X.; Cho, Y. Characterization of Microstructural Evolution by Ultrasonic Nonlinear Parameters Adjusted by Attenuation Factor. *Metals* **2019**, *9*, 271. [CrossRef]
26. Rauter, N.; Lammering, R. Numerical simulation of elastic wave propagation in isotropic media considering material and geometrical nonlinearities. *Smart Mater. Struct.* **2015**, *24*, 045027. [CrossRef]
27. Li, W.B.; Deng, X.; Xiang, Y.X. Review on second-harmonic generation of ultrasonic guided waves in solid media (I): Theoretical analyses. *Chin. Phys. B* **2017**, *26*, 114302. [CrossRef]
28. Matlack, K.H.; Kim, J.Y.; Jacobs, L.J.; Qu, J. Experimental characterization of efficient second harmonic generation of lamb wave modes in a nonlinear elastic isotropic plate. *J. Appl. Phys.* **2011**, *109*, 014905. [CrossRef]
29. Hayashi, T.; Song, W.J.; Rose, J.L. Guided wave dispersion curves for a bar with an arbitrary cross-section, a rod and rail example. *Ultrasonics* **2003**, *41*, 175–183. [CrossRef]
30. Yan, F. Ultrasonic Guided Wave Phased Array for Isotropic and Anisotropic Plates. Ph.D. Thesis, Department of Engineering Science and Mechanics, Penn State University, State College, PA, USA, 2008.
31. Yamada, Y. *Materials for Springs*; Japan Society of Spring Engineers: Tokyo, Japan, 2007; ISBN 978-3-540-73811-4.
32. Rose, J.L. *Ultrasonic Waves in Solid Media*; Cambridge University press: Cambridge, MA, USA, 2014.
33. Bussloti, R.; Canale, L.C.F.; Totten, G. Delta Ferrite in Heat Treated Bolts—Characterization and Consequences. In Proceedings of the Heat Treat 2013 American Society for Metals, Indianapolis, IN, USA, 16–18 September 2013.
34. Michihiko, A.; Noritoshi, T. Analysis of Load, Stress and Deflection in Nakamura-Type Rotating-bending fatigue Test. *Trans. Jpn. Soc. Spring Eng.* **1992**, *37*, 59–64.